Chemical Science

EDGE ARTICLE

View Article Online
View Journal | View Issue

Cite this: *Chem. Sci.*, 2016, 7, 5821

Thin film transfer for the fabrication of tantalum nitride photoelectrodes with controllable layered structures for water splitting†

Chizhong Wang,[a] Takashi Hisatomi,[ab] Tsutomu Minegishi,[abc] Mamiko Nakabayashi,[d] Naoya Shibata,[d] Masao Katayama[ab] and Kazunari Domen*[ab]

Received 22nd April 2016
Accepted 25th May 2016

DOI: 10.1039/c6sc01763k

www.rsc.org/chemicalscience

The fabrication of semiconductor films on conductive substrates is vital to the production of high-performance electrodes for photoelectrochemical (PEC) water splitting. In this work, a thin film transfer method was developed to produce Ta_3N_5 film photoanodes for PEC water oxidation. Phase-pure Ta_3N_5 thin films were formed on inert Si substrates *via* magnetron sputtering of Ta films, followed by oxidation and subsequent nitridation in a flow of gaseous NH_3. The resulting porous Ta_3N_5 films were uniformly transferred from the Si substrates using metallic layers that allowed ohmic contact at the Ta_3N_5 film/metal interface. This film transfer method enables control over the film thicknesses and layered structures of the Ta_3N_5 photoanodes. Following modification with a $Co(OH)_x$ layer acting as an oxygen-evolution catalyst, a Ta_3N_5 photoanode with a NbN_x interlayer exhibited a photocurrent of 3.5 mA cm^{-2} at 1.23 V *vs.* RHE under a simulated AM 1.5G light, a value 1.7 times that generated by a photoanode without interlayers. The present film transfer method is potentially applicable to the development of semiconductor thin films for efficient PEC energy conversion.

Open Access Article. Published on 25 mayo 2016. Downloaded on 05/10/2024 4:18:51.
This article is licensed under a Creative Commons Attribution-NonCommercial 3.0 Unported Licence.

Introduction

The conversion of solar energy to hydrogen by photoelectrochemical (PEC) water splitting is a promising approach to meeting the increasing demand for sustainable energy.[1,2] In a typical p/n PEC device, the photoelectrode is composed of a semiconductor layer for light harvesting and a back contact layer to conduct light-induced majority charge carriers to a counter electrode.[3,4] (Oxy)nitride materials, such as Ta_3N_5, $(Ga_{1-x}Zn_x)(N_{1-x}O_x)$, $BaTaO_2N$, and $LaTiO_2N$, absorb over a sufficient range of visible light wavelengths in the solar spectrum and have suitable band edge positions to allow for efficient PEC water oxidation.[5–8] Several synthesis methods have been developed to configure (oxy)nitride photoelectrodes, including high-temperature nitridation of oxide layers,[9–13] reactive magnetron sputtering,[14] electrophoretic deposition,[15] and particle transfer.[7,8,16]

Ta_3N_5, having a bandgap of 2.1 eV,[17] is the nitride material most commonly studied for PEC water splitting, because it is a simple binary nitride and has demonstrated activity for PEC water oxidation. Powder-based Ta_3N_5 photoelectrodes can be fabricated on transparent conductive oxide layers by electrophoretic deposition.[18] However, such photoelectrodes suffer from inefficient electron transfer across thick particulate Ta_3N_5 layers and at the interface between the Ta_3N_5 and the conductive substrate.[19–22] In contrast, Ta_3N_5 photoelectrodes grown on conductive substrates (typically Ta foils) in the form of thin films or nanorods have been reported to exhibit high photocurrent and negative onset potentials.[23–25] Unfortunately, opportunities to enhance the PEC activity by tuning the film thickness and introducing multi-layer structures are restricted owing to the insufficient durability of Ta metal substrates during high-temperature treatments. The Ta_3N_5 layer is prone to reduction to Ta-rich species (such as Ta_5N_6, TaN and Ta_2N) and to the formation of impurity interfacial layers resulting from the thermal diffusion of Ta from the substrate during the nitridation process.[26–28]

A particle transfer process has recently been developed to fabricate particulate Ta_3N_5 photoelectrodes with excellent mechanical and electric contacts by separating the nitridation process and the deposition of contact layers.[8,16] Inspired by this method, we present a thin film transfer method for Ta_3N_5 photoelectrodes to realise precise control in film thickness and

[a]Department of Chemical System Engineering, School of Engineering, The University of Tokyo, 7-3-1 Hongo, Bunkyo-ku, 113-8656 Tokyo, Japan. E-mail: domen@chemsys.t.u-tokyo.ac.jp; Fax: +81 3 5841 8838; Tel: +81 3 5841 1148

[b]Japan Technological Research Association of Artificial Photosynthetic Chemical Process (ARPChem), 2-11-9 Iwamotocho, Chiyoda-ku, 101-0032 Tokyo, Japan

[c]Japan Science and Technology Agency/Precursory Research for Embryonic Science and Technology (JST/PRESTO), Kawaguchi Center Building, 4-1-8, Honcho, Kawaguchi-shi, 332-0012 Saitama, Japan

[d]Institute of Engineering Innovation, The University of Tokyo, 2-11-16 Yayoi, Bunkyo-ku, 113-8656 Tokyo, Japan

† Electronic supplementary information (ESI) available. See DOI: 10.1039/c6sc01763k

synthesis parameters. Using this approach, we have demonstrated that various metallic and semiconductor layers can be introduced as back contacts to improve the PEC performance of Ta_3N_5 photoanodes.

Experimental section

Materials preparation

The procedure used to synthesize Ta_3N_5 by thin film transfer is presented in Fig. 1. Single-crystalline Si wafers (Nilaco Co.) were cut into specimens with dimensions of 1 × 1 cm. These Si substrates were then treated by sequential sonication in acetone, 2-propanol and Milli-Q water (18.2 mΩ cm), and the cleaned Si substrates were directly used, without HF etching to remove the surface native SiO_2. Thin Ta films, with thicknesses ranging from 150 to 800 nm, were deposited on these Si substrates by radio-frequency (RF) magnetron sputtering (ULVAC, MNS-2000-RFG3) at a substrate temperature of 500 °C. The working pressure and the output power of the Ar plasma during this process were 1.0×10^{-1} Pa and 100 W, respectively. The deposition rate of the Ta film was 25 nm min^{-1}. The resulting Ta/Si samples were oxidised in a muffle furnace at 700 °C for 2 h to form Ta_2O_5 films, and these Ta_2O_5/Si specimens were subsequently nitrided in a flow of gaseous NH_3 (100 sccm) at 900 °C for 2 h to produce Ta_3N_5 thin films on the Si substrates. Ta (150 nm) and Ti (approximately 5 μm) layers were then sputtered on top of the as-nitrided Ta_3N_5 thin films. In some cases, the Ta layer was replaced with Nb, Ti, Zr (containing 4.5% Hf) or Mg and different contact materials were investigated, as described in the ESI.† The Ta_3N_5/Ta/Ti films could be completely peeled away from the Si substrates by mechanical exfoliation. The transferred films were cleaned with an HF/HNO_3/H_2O (1/2/7, v/v) solution for 10 s. Subsequently, the back side of each Ta_3N_5/Ta/Ti sample was attached to a glass plate with carbon tape and connected to an electrical wire using indium solder. The electrode area exposed to the electrolyte solution was defined by applying a water-proof epoxy resin, and the typical exposed electrode area was approximately 0.2 cm^2.

A layer of $Co(OH)_x$ was deposited on the surface of each Ta_3N_5 photoelectrode prior to the photoelectrochemical (PEC) measurements. An aqueous 2.5 mL NaOH (50 mM) solution was added to 10 mL of an aqueous $Co(NO_3)_2$ (6.3 mM) solution, and the as-prepared Ta_3N_5 photoelectrode was immersed in the mixture for 1 h. As the initial blue solution gradually transitioned to a yellow colloidal suspension, a thin layer of $Co(OH)_x$ was formed on the surface of the electrode.

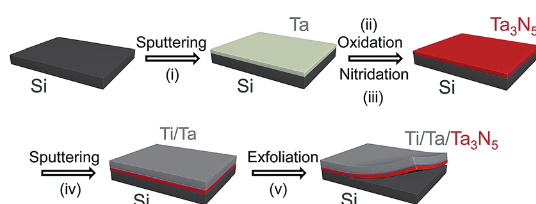

Fig. 1 Schematic depicting the processes involved in the thin film transfer method. (i) A Ta thin film is deposited on the Si substrate by sputtering, (ii) the Ta film is oxidised to Ta_2O_5 on the Si substrate, (iii) the Ta_2O_5/Si is converted to Ta_3N_5/Si by nitridation in a flow of gaseous NH_3, (iv) Ta and Ti layers are sequentially sputtered on the surface of the Ta_3N_5/Si, and (v) the resulting Ta_3N_5/Ta/Ti is mechanically exfoliated from the Si substrate and used as a photoelectrode.

Characterization

Scanning electron microscopy (SEM; S-4700, Hitachi), scanning transmission electron microscopy and transmission electron microscopy (STEM, TEM; JEM-2800, JEOL) in conjunction with energy-dispersive X-ray spectroscopy (EDS; EX-24055JGT, JEOL) were used to characterise the morphologies and cross-sectional structures of the Ta_3N_5 thin films. X-ray diffraction (XRD; Rigaku Ultima III) patterns were acquired using Cu Kα radiation (λ = 0.15405 nm, 40 mV and 40 mA) and X-ray photoelectron spectroscopy (XPS; JEOL, JPS-90SX) was performed with Mg Kα radiation (8 kV and 10 mA).

Photoelectrochemical measurements

The PEC properties of the Ta_3N_5 photoanodes were assessed in a three-electrode cell controlled by a potentiostat (Hokuto Denko, HSV-110). An Ag/AgCl (in saturated KCl aq.) electrode and a Pt wire were used as the reference and counter electrodes, respectively. The potential against the Ag/AgCl reference electrode ($E_{Ag/AgCl}$) was converted to the potential with respect to a reversible hydrogen electrode (E_{RHE}) using the Nernst equation below.

$$E_{RHE} = E_{Ag/AgCl} + 0.197 \text{ V} + 0.059 \times \text{pH} \quad (1)$$

PEC measurements were performed in an aqueous solution of potassium phosphate (KPi, 0.5 M, pH 13) under a simulated AM 1.5G light source (San-EI Electric, XES-40S2-CE). The H_2 and O_2 gas yields from the counter electrode and a Ta_3N_5 photoanode held at 1.23 V *vs.* RHE were accumulated in an air-tight, three-electrode PEC cell and quantified using a micro gas chromatograph (Agilent, 3000A, Micro GC).

Results and discussion

Fig. 2 presents XRD patterns for the thin film samples before nitridation, after nitridation, and after film transfer. Fig. 2(a) demonstrates that a crystalline Ta_2O_5 film was formed by oxidising the metallic Ta film at 700 °C, while Fig. 2(b) shows that a Ta_3N_5 film with an orthorhombic phase was formed on the Si substrate by nitridation at 900 °C. The crystalline Ta_3N_5 films were evidently preserved during the film transfer process (Fig. 2(c)). Ta_2N and Ta_5N_6, which are both typical impurity phases in Ta_3N_5 films grown on Ta metal substrates,[26,27] were not observed in our Ta_3N_5 films having thicknesses of 570, 1120, and 1620 nm, as shown in Fig. S1 in the ESI.† This suggests that reduction of the Ta_3N_5 phase during the nitridation process was inhibited owing to the absence of the underlying Ta metal. Complete transformation to Ta_3N_5 was achieved even in the case of the especially thick Ta_3N_5 films (>1000 nm). This was likely due to the formation of a porous structure that facilitated penetration of N or NH species throughout the film.

Open Access Article. Published on 25 mayo 2016. Downloaded on 05/10/2024 4:18:51. This article is licensed under a Creative Commons Attribution-NonCommercial 3.0 Unported Licence.

 This journal is © The Royal Society of Chemistry 2016

Open Access Article. Published on 25 mayo 2016. Downloaded on 05/10/2024 4:18:51.
This article is licensed under a Creative Commons Attribution-NonCommercial 3.0 Unported Licence.

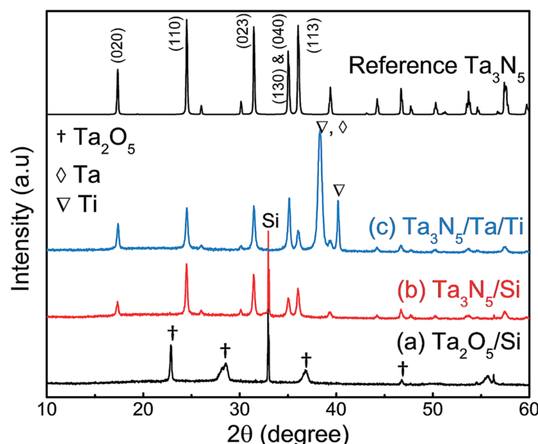

Fig. 2 XRD patterns for (a) Ta_2O_5/Si and (b) Ta_3N_5/Si obtained from the nitridation of Ta_2O_5/Si, and (c) Ta_3N_5/Ta/Ti after the transfer process. The standard pattern for the Ta_3N_5 phase (PDF# 89-5200) is displayed at the top as a reference.

Fig. 3(a) shows a cross-sectional SEM image of a Ta_3N_5 film on a Si substrate. This porous Ta_3N_5 film was formed by nitridation as the three O^{2-} anions in the original Ta_2O_5 film were replaced by two N^{3-} anions. From the cross-sectional images (Fig. 3(b) and (c)), it is evident that the thickness of the Ta_3N_5 film (570 nm) remained unchanged during the film transfer process. The multi-layer Ta_3N_5/Ta/Ti structure was further confirmed by the cross-sectional EDS maps presented in Fig. 3(d) and (e). Because the sputtered Ta/Ti layer resulted in rigid contact with the Ta_3N_5 layer, the Ta_3N_5 film was readily exfoliated from the Si substrate without damaging the layered structure of the Ta_3N_5/Ta/Ti film. However, Ta_3N_5 films thinner than 300 nm could not be peeled away from the Si substrate without breaking. It is believed that the presence of significant porosity at the film/substrate interface plays a key role in successful film transfer, given the correlation between the porosity and thickness of Ta_3N_5 thin films.[19] The metallic Ta and Ti layers acted as a back contact and a conductive support for the Ta_3N_5 films, respectively. The transferred Ta_3N_5 film was flexible (Fig. 3(f)) and had a rough surface originating from the porosity of the Ta_3N_5 (Fig. 3(g)). XPS analysis of the Ta_3N_5 films before and after transfer (Fig. S2†) revealed that no Si species were present on the surface of the Ta_3N_5 film after thin film transfer. This result demonstrates a lack of Si diffusion into the bulk of the Ta_3N_5 film, owing to the stability of the Si substrates during the high temperature nitridation.

In order to examine the structural properties of the Ta_3N_5 film, a dark-field (DF) STEM image (Fig. 2(h)) of a cross section close to the Ta_3N_5/Ta interface was acquired. The bright contrast in this DF-STEM image indicates a highly porous structure for the transferred Ta_3N_5 film. The average size of the pores between the Ta_3N_5 grains was approximately 20 nm, and thus was likely responsible for the high surface area of the Ta_3N_5 photoelectrodes. The average grain sizes of Ta_3N_5 crystals were estimated from the zone-axis TEM image (Fig. 2(i)) to be in the range of 20 to 50 nm, a value that is much smaller than the film thickness (570 nm). The TEM fast Fourier transform (FFT) diffraction patterns also demonstrate disorder in the

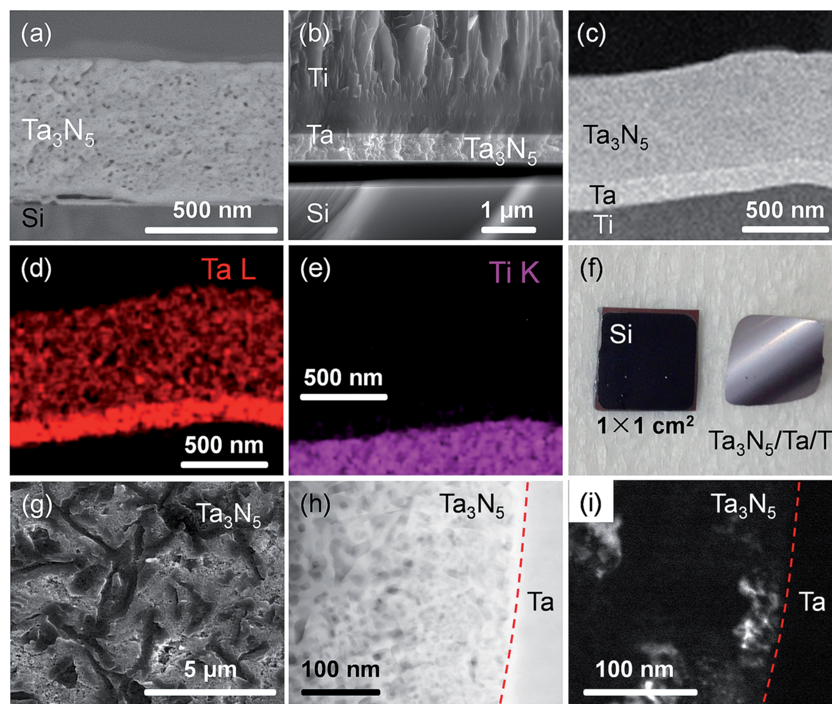

Fig. 3 Cross-sectional SEM images of (a) Ta_3N_5/Si and (b) Ti/Ta/Ta_3N_5/Si, (c) cross-sectional STEM image of transferred Ta_3N_5/Ta/Ti, EDS maps for (d) Ta and (e) Ti taken from the STEM image in panel (c), (f) digital photographs of a Ta_3N_5/Ta/Ti sample transferred from a Si substrate, (g) top-view SEM image of a Ta_3N_5/Ta/Ti sample, and dark-field (h) STEM and (i) zone-axis TEM images of a Ta_3N_5/Ta/Ti sample near the Ta_3N_5/Ta interface.

Open Access Article. Published on 25 mayo 2016. Downloaded on 05/10/2024 4:18:51.
This article is licensed under a Creative Commons Attribution-NonCommercial 3.0 Unported Licence.

arrangement of the Ta_3N_5 grains (Fig. S3†). Hence, a number of grain boundaries were present in the Ta_3N_5 film. However, the thin film was in intimate contact with the polycrystalline Ta layer prepared by magnetron sputtering. Owing to the matching of the work function of metallic Ta (4.3 eV)[29] and the flat band potential of the Ta_3N_5 electrode (0.02 V *vs.* RHE, Fig. S4†), an ohmic contact was expected to be present at the Ta_3N_5/Ta interface. As a result, the energy barrier for the transport of photogenerated electrons across the Ta_3N_5/Ta interface was minimized.

Current–potential curves for Ta_3N_5 photoanodes with film thicknesses of 570, 1120 and 1620 nm were obtained under simulated AM 1.5G light and are presented in Fig. 4(a). A photocurrent density of 2.0 mA cm^{-2} at 1.23 V *vs.* RHE was observed in the case of the Ta_3N_5(570 nm)/Ta/Ti photoelectrode modified with a cobalt-based oxygen-evolution catalyst. The faradaic efficiency for PEC water oxidation reaction was determined by quantifying the O_2 evolved at the Ta_3N_5/Ta/Ti photoanode held at 1.23 V *vs.* RHE and the H_2 evolved at the Pt counter electrode by gas chromatography (Fig. 4(b)). The faradaic efficiency of almost unity indicates that the photoanodic current generated by the Ta_3N_5 photoelectrode is primarily attributable to the O_2 evolution process. The incident photon-to-current conversion efficiency (IPCE) spectrum (Fig. S5†) demonstrates that the Ta_3N_5 film photoanodes were capable of utilising visible light up to 600 nm, corresponding to the bandgap of Ta_3N_5 (2.1 eV), for PEC water oxidation. However, because of the porous nature of the Ta_3N_5 films, the photoelectrode surface was not fully covered with the $Co(OH)_x$ layer (Fig. S6†). As a result, the O_2 evolution rate decreased gradually over time owing to the photocorrosion of the Ta_3N_5 films.

A significant decrease in the photocurrent density was associated with increases in the film thicknesses of the Ta_3N_5 photoelectrodes. The probability of charge carrier recombination in thicker Ta_3N_5 films is expected to be higher, given the large number of grain boundaries acting as electron–hole recombination centres and the long diffusion distances for both holes and electrons. It should be noted that Ta_3N_5 films thinner than 300 nm could not be prepared by film transfer from Si substrates as described above.[19] Therefore, a film thickness of approximately 600 nm was the optimum value for the Ta_3N_5 photoanodes prepared by thin film transfer. This thickness is consistent with the layer thickness reported for Ta_3N_5 photoelectrodes with exhibiting superior PEC performance.[19,24]

The thin film transfer method allows tuning of the thickness of the Ta_3N_5 film to arbitrary values above approximately 550 nm. Another and potentially more important feature of the film transfer technique is the possibility of obtaining the desired multi-layer structure in the Ta_3N_5 film. It is conceptually possible to introduce doping, catalytic, protective, and/or sacrificial template layers at the front and/or rear sides of the Ta_3N_5 film by depositing such functional layers before and/or after formation of either the Ta or Ta_2O_5 layers. It is also feasible to use materials other than Ta, such as metals, sulphides, and nitrides, as contact layers after the nitridation. As an example, current–potential curves for Ta_3N_5 photoelectrodes with different metallic contact layers (Ta, Nb, Ti, Zr and Mg) are shown in Fig. 5(a). It was found that Ta_3N_5 photoelectrodes with Ta and Nb back contacts showed higher photocurrents than those with Mg and Zr back contacts although all the metallic layers were expected to form an ohmic contact with the Ta_3N_5 films. A Mg or Zr contact layer with small work function (Table S1 in ESI†) was probably too sensitive to oxygen to form an ideal ohmic junction, resulting in a poor PEC performance. In addition, NbN_x, TiN_x and CdS were introduced as back contact materials for Ta_3N_5 photoelectrodes (Fig. 5(b) and S7†). A Ta_3N_5/NbN_x/Ta photoelectrode with a NbN_x back contact generated a higher current density (3.5 ± 0.2 mA cm^{-2} at 1.23 V *vs.* RHE) than a Ta_3N_5/Ta photoelectrode (2.2 ± 0.2 mA cm^{-2}), as shown in Fig. S8,† while TiN_x and CdS back contacts lowered the PEC activity. The photocurrent of the Ta_3N_5/NbN_x/Ta photoanode decayed with time, similarly to the Ta_3N_5/NbN_x/Ta photoanode, because the interlayer did not suppress photocorrosion of the Ta_3N_5 surface. In addition, the effects of the back contact materials on the properties of the Ta_3N_5 films are not fully understood at present. However, it is clear that certain back contact materials can promote PEC oxygen evolution on Ta_3N_5 thin films. In future work, this film transfer process is expected to allow clarification of the promotional effect of interlayers on the PEC properties of Ta_3N_5 films by taking advantage of the controllability of the layered structure.

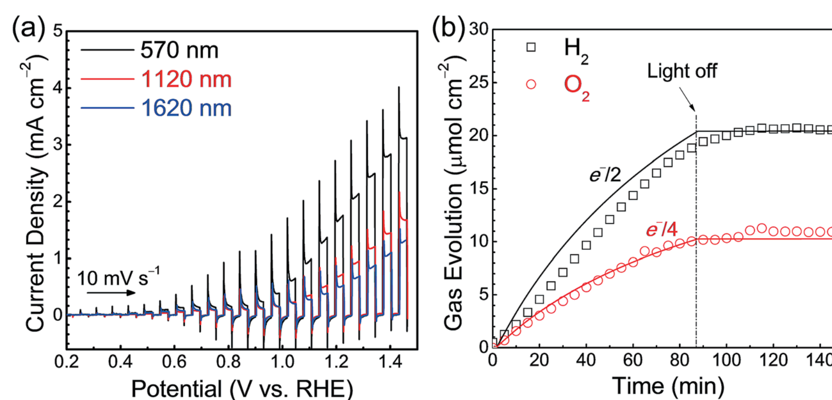

Fig. 4 (a) Current–potential curves obtained from Ta_3N_5 photoanodes with different film thicknesses under simulated AM 1.5G light, and (b) time course of O_2 (open circles) and H_2 (open squares) gas evolution from a Ta_3N_5(570 nm)/Ta/Ti photoanode held at 1.23 V *vs.* RHE and a Pt counter electrode, respectively, under simulated AM 1.5G light. Solid curves represent the total charges estimated from the photocurrent.

This journal is © The Royal Society of Chemistry 2016

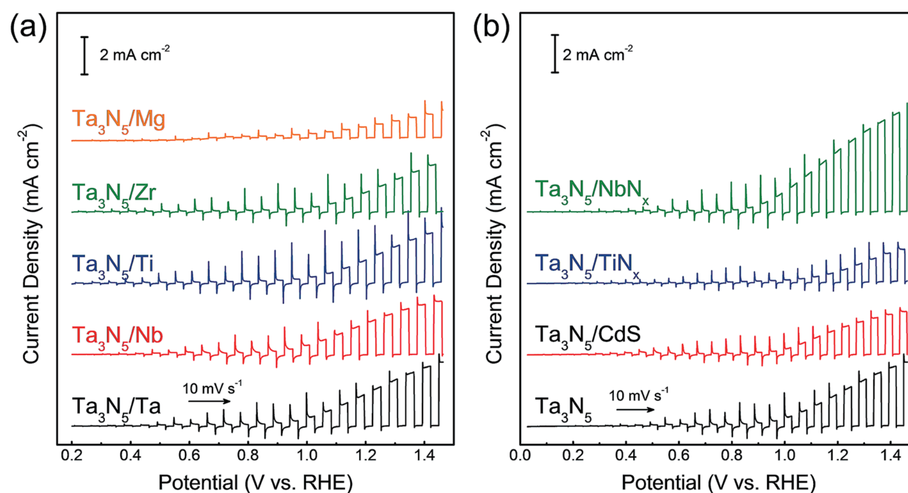

Fig. 5 Current–potential curves obtained from Ta_3N_5 photoanodes with different back contact layers. (a) Ta_3N_5/M/Ti (M = Ta, Nb, Ti, Zr and Mg), and (b) Ta_3N_5/N/Ta/Ti (N = NbN_x, TiN_x and CdS).

Open Access Article. Published on 25 mayo 2016. Downloaded on 05/10/2024 4:18:51. This article is licensed under a Creative Commons Attribution-NonCommercial 3.0 Unported Licence.

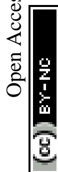

Conclusions

A thin film transfer method for the fabrication of Ta_3N_5 thin films having different thicknesses and back contact layers has been demonstrated. The inertness of the Si substrates allowed the synthesis of pure, crystalline Ta_3N_5 films *via* the thermal nitridation of sputtered Ta films, and also resulted in weak adhesion at the Ta_3N_5/Si interface that promoted the film transfer process. This new preparation method allows optimization of the PEC performance of Ta_3N_5 thin film photoanodes by controlling the film thickness. Ta_3N_5(570 nm)/Ta/Ti photoanodes generated a photocurrent of 2.0 mA cm^{-2} at 1.23 V *vs.* RHE under simulated AM 1.5G light, while thicker films produced lower photocurrents because of the longer charge carrier migration distances and the greater concentration of grain boundaries. The photocurrent at 1.23 V *vs.* RHE could be further enhanced to 3.5 mA cm^{-2} by modification of the back contact layer applied to the transferred Ta_3N_5 film.

This film transfer procedure circumvents current strict requirements for the conductive substrates that can be employed during vigorous annealing treatments, enabling the preparation and the transfer of semiconductor thin films from various inert substrates. Therefore, the new fabrication strategy presented herein has the potential to allow the preparation of thin film photoelectrodes composed of materials such as α-Fe_2O_3, $BiVO_4$ and $BaTaO_2N$ for applications in PEC water splitting and/or PEC solar cells.

Acknowledgements

This work was financially supported by Grants-in-Aid for Specially Promoted Research (No. 23000009), for Young Scientists (A) (No. 15H05494) and Young Scientists (B) (No. 5K17895) of Japan Society for the Promotion of Science (JSPS). This work was partly supported by the Artificial Photosynthesis Project (ARPChem) of the New Energy and Industrial Technology Development Organization (NEDO). Part of this work was conducted at the Research Hub for Advanced Nano Characterization at the University of Tokyo, under the support of the "Nanotechnology Platform" (project No. 12024046) of the Ministry of Education, Culture, Sports, Science and Technology (MEXT), Japan. The authors thank Dr Qian Wang, Dr Miao Zhong, Dr Taro Yamada and Mr Yutaka Sasaki in the University of Tokyo for SEM characterisation and discussions.

References

1 M. Grätzel, *Nature*, 2001, **414**, 338–344.
2 A. Fujishima and K. Honda, *Nature*, 1972, **238**, 37–38.
3 A. J. Nozik, *Annu. Rev. Phys. Chem.*, 1978, **29**, 189–222.
4 M. G. Walter, E. L. Warren, J. R. McKone, S. W. Boettcher, Q. Mi, E. A. Santori and N. S. Lewis, *Chem. Rev.*, 2010, **110**, 6446–6473.
5 T. Hisatomi, J. Kubota and K. Domen, *Chem. Soc. Rev.*, 2014, **43**, 7520–7535.
6 M. Zhong, Y. Ma, P. Oleynikov, K. Domen and J.-J. Delaunay, *Energy Environ. Sci.*, 2014, **7**, 1693–1699.
7 K. Ueda, T. Minegishi, J. Clune, M. Nakabayashi, T. Hisatomi, H. Nishiyama, M. Katayama, N. Shibata, J. Kubota, T. Yamada and K. Domen, *J. Am. Chem. Soc.*, 2015, **137**, 2227–2230.
8 T. Minegishi, N. Nishimura, J. Kubota and K. Domen, *Chem. Sci.*, 2013, **4**, 1120–1124.
9 H. X. Dang, N. T. Hahn, H. S. Park, A. J. Bard and C. B. Mullins, *J. Phys. Chem. C*, 2012, **116**, 19225–19232.
10 S. Khan, M. J. M. Zapata, M. B. Pereira, R. V. Goncalves, L. Strizik, J. Dupont, M. J. L. Santos and S. R. Teixeira, *Phys. Chem. Chem. Phys.*, 2015, **17**, 23952–23962.
11 C. Wang, T. Hisatomi, T. Minegishi, Q. Wang, M. Zhong, M. Katayama, J. Kubota and K. Domen, *J. Phys. Chem. C*, 2016, DOI: 10.1021/acs.jpcc.5b11564.
12 G. J. Liu, J. Y. Shi, F. X. Zhang, Z. Chen, J. F. Han, C. M. Ding, S. S. Chen, Z. L. Wang, H. X. Han and C. Li, *Angew. Chem., Int. Ed.*, 2014, **53**, 7295–7299.

Open Access Article. Published on 25 mayo 2016. Downloaded on 05/10/2024 4:18:51.
This article is licensed under a Creative Commons Attribution-NonCommercial 3.0 Unported Licence.

13 M. X. Li, W. J. Luo, D. P. Cao, X. Zhao, Z. S. Li, T. Yu and Z. G. Zou, *Angew. Chem., Int. Ed.*, 2013, **52**, 11016–11020.
14 D. Yokoyama, H. Hashiguchi, K. Maeda, T. Minegishi, T. Takata, R. Abe, J. Kubota and K. Domen, *Thin Solid Films*, 2011, **519**, 2087–2092.
15 M. Higashi, K. Domen and R. Abe, *J. Am. Chem. Soc.*, 2013, **135**, 10238–10241.
16 J. Seo, T. Takata, M. Nakabayashi, T. Hisatomi, N. Shibata, T. Minegishi and K. Domen, *J. Am. Chem. Soc.*, 2015, **137**, 12780–12783.
17 W. J. Chun, A. Ishikawa, H. Fujisawa, T. Takata, J. N. Kondo, M. Hara, M. Kawai, Y. Matsumoto and K. Domen, *J. Phys. Chem. B*, 2003, **107**, 1798–1803.
18 M. Higashi, K. Domen and R. Abe, *Energy Environ. Sci.*, 2011, **4**, 4138–4147.
19 B. A. Pinaud, P. C. K. Vesborg and T. F. Jaramillo, *J. Phys. Chem. C*, 2012, **116**, 15918–15924.
20 A. Dabirian and R. van de Krol, *Chem. Mater.*, 2015, **27**, 708–715.
21 A. Ziani, E. Nurlaela, D. S. Dhawale, D. A. Silva, E. Alarousu, O. F. Mohammed and K. Takanabe, *Phys. Chem. Chem. Phys.*, 2015, **17**, 2670–2677.
22 J. M. Morbec, I. Narkeviciute, T. F. Jaramillo and G. Galli, *Phys. Rev. B*, 2014, **90**, 155204.
23 G. Liu, S. Ye, P. Yan, F. Xiong, P. Fu, Z. Wang, Z. Chen, J. Shi and C. Li, *Energy Environ. Sci.*, 2016, **9**, 1327–1334.
24 Y. Li, L. Zhang, A. Torres-Pardo, J. M. González-Calbet, Y. Ma, P. Oleynikov, O. Terasaki, S. Asahina, M. Shima, D. Cha, L. Zhao, K. Takanabe, J. Kubota and K. Domen, *Nat. Commun.*, 2013, **4**, 2566.
25 C. Zhen, L. Wang, G. Liu, G. Q. Lu and H.-M. Cheng, *Chem. Commun.*, 2013, **49**, 3019–3021.
26 B. A. Pinaud, A. Vailionis and T. F. Jaramillo, *Chem. Mater.*, 2014, **26**, 1576–1582.
27 Y. Li, T. Takata, D. Cha, K. Takanabe, T. Minegishi, J. Kubota and K. Domen, *Adv. Mater.*, 2013, **25**, 125–131.
28 T. Nobuzo, *Jpn. J. Appl. Phys.*, 1971, **10**, 248–259.
29 H. L. Skriver and N. M. Rosengaard, *Phys. Rev. B: Condens. Matter Mater. Phys.*, 1992, **46**, 7157–7168.

This journal is © The Royal Society of Chemistry 2016